

# A Dynamic Cooler Model for Cement Clinker Production

Jan Lorenz Svensen<sup>1,2</sup>, Wilson Ricardo Leal da Silva<sup>2</sup>, Javier Pigazo Merino<sup>2</sup>,  
Dinesh Sampath<sup>2</sup> and John Bagterp Jørgensen<sup>1</sup>

**Abstract**—We present a 2D model for a grate belt cooler in the pyro-section of a cement plant. The model is formulated as an index-1 differential-algebraic equation (DAE) model based on first engineering principles. The model systematically integrates thermo-physical aspects, transport phenomena, reaction kinetics, mass and energy balances, and algebraic volume and energy relations. The model is used for dynamic simulation of the cooler and the paper provides dynamic and steady-state simulation results matching the expected behavior. The cooler model is one part of a full pyro-section model for dynamical simulations. The model can serve as a basis for the design of optimization and control systems towards improving energy efficiency and CO<sub>2</sub> emission.

## I. INTRODUCTION

The manufacturing of cement corresponds to 8% of the global CO<sub>2</sub> emissions [1]. A main source of these emissions comes from the production of cement clinker. On the transition towards zero CO<sub>2</sub> emissions, optimization, control, and digital solutions are important approaches just as process modification for carbon capture and alternative materials are. For the development of digital, control, and optimization approaches for the pyro-process, and the cement plants in general, dynamic simulations are a requirement.

Fig. 1 illustrates the pyro-process of cement clinker production. The process consists of a pre-heating tower of cyclones, a calciner, a rotary kiln, and a cooler. In this paper, we provide a mathematical model for dynamic simulations of the cooler. We specifically consider a grate belt cooler. The cooler model is useful for the design of control and optimization systems for both heat recirculation and clinker quality, critical for the operation of cement plants.

In the existing literature on models, Metzger modeled the cooler as a dynamic 1D model of energy balances without a radiation term [2]. Cui et al suggested a steady-state 2D model for the energy balances with porosity, though without radiation or mass balances [3]. Mujumdar et al suggested a steady-state 2D model for the energy balance with applied porosity and a 1D mass balance model for the overall mass flow [4].

In comparison, we provide a mathematical 2D model for dynamic simulations of the cooler, including both mass and energy balances for the material and gas content. The model describes the material compositions, flows, and heat

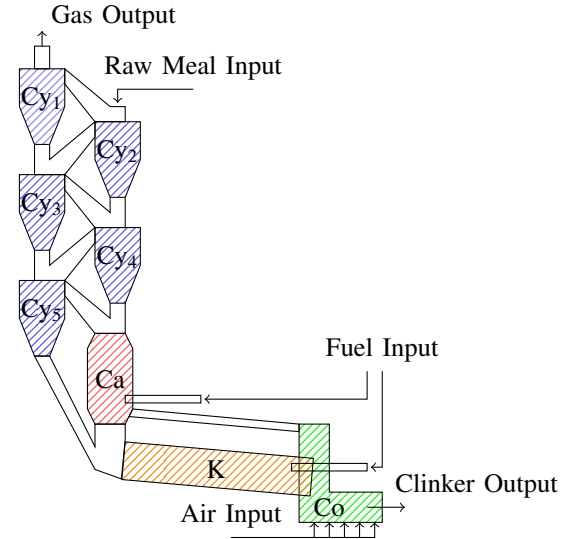


Fig. 1: The pyro-section for clinker production in a cement plant consists of preheating tower of cyclones (Cy), a calciner (Ca), a rotary kiln (K), and a cooler (Co).

exchanges based on rigorous thermo-physical properties and kinetic expressions. The model is formulated as a system of index-1 differential algebraic equations (DAEs), using a novel systematic modeling methodology that integrates thermo-physical properties, transport phenomena, and stoichiometry and kinetics with mass and energy balances. The modeling approach allows for simple formulations of models without the need of supplementary assumptions, e.g. assuming properties like heat capacity being constant. Models of the complementary parts of the pyro-process can be found in [5] and [6] for rotary kiln and calciner, respectively. The literature provides references on industrial cooler operation and design practices [7][8][9].

This paper is organized as follows. Section II presents the cooler, while Section III describes the mathematical model for the cooler. Section IV presents simulation results and Section V provides the conclusions of the paper.

## II. THE COOLER

In clinker production, the main purpose of the cooler is to stabilize the produced cement clinker by rapid cooling (quenching). As part of the clinker production process, Belite (dicalcium silicate, C<sub>2</sub>S) reacts above 1300°C to form Alite (tricalcium silicate, C<sub>3</sub>S), a main source of early cement strength. If the clinker cooling is too slow, Alite converts

\*This work was supported by Innovation Fund Denmark, Ref. 2053-00012B

<sup>1</sup> DTU Compute, Department of Applied Mathematics and Computer Science, Technical University of Denmark, 2800 Lyngby, Denmark jlsv@dtu.dk, jbj@dtu.dk

<sup>2</sup> FLSmidth A/S, 2500, Valby, Denmark wld@flsmidth.com

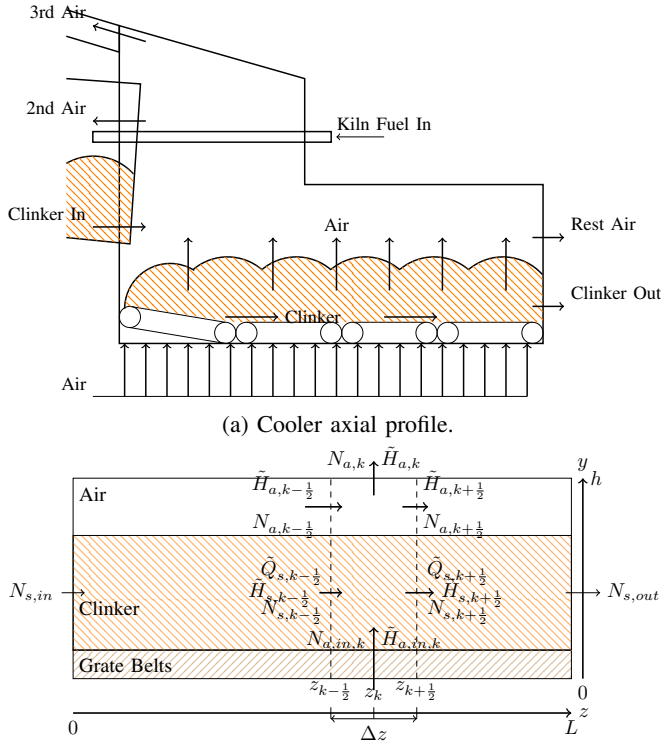
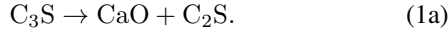


Fig. 2: Cooler axial profile.

back into Belite.



A second purpose of the cooler is the recirculation of heat to improve fuel efficiency of the entire production. Several cooler types exist, e.g. rotary, planetary, shaft or grate belts [7]. Fig. 2a illustrates how clinker and air move in a grate belt cooler. The clinker enters from the kiln and is transported through the cooler by a grate belt. Cool air is blown through the grate belt from below to cool the clinker, the air is afterward either released or recirculated back into the process as secondary air (2nd air) and tertiary air (3rd air) flows for the heating of the kiln and calciner sections. The entering clinker mass typically has a temperature of 1300-1450°C, while the exiting clinker temperature is around 100-150°C [7], above the ambient temperature. The Alite decomposition into Belite in (1a) happens between 900°C and 1250°C [10].

### III. A MATHEMATICAL COOLER MODEL

For modeling the cooler as an index-1 DAE system, we consider the molar concentrations of each compound,  $C$ , and the internal energy densities of each phase,  $\hat{U}$ , as the states,  $x$ . The algebraic variables,  $y$ , are the phase temperatures,  $T$ , and the pressure,  $P$ . The resulting model reads:

$$\partial_t x = f(x, y; p), \quad x = [C; \hat{U}], \quad (2a)$$

$$0 = g(x, y; p), \quad y = [T; P], \quad (2b)$$

with  $p$  being the system parameters. The model considers two phases, the solid clinker materials and the air given by the subscripts  $s$  and  $a$ . The model is formulated using a systematic modeling methodology that integrates A) algebraic relations, B) mass and energy balances, C) thermo-physical properties, D) stoichiometry and kinetics, and E) transport phenomena.

We use a finite-volume approach to describe the cooler in  $nv$  segments of length  $\Delta z = L/nv$  along its length. Fig. 2b illustrates how the cooler model is segmented, with a total height  $h$ , width  $w$ , and length  $L$ . We define the molar concentration vector,  $C$ , as mole per segment volume  $V_\Delta(k) = wh\Delta z$ , and assume all gasses are ideal.

The standard cement chemist notation is used for the compounds:  $(\text{CaO})_2\text{SiO}_2$  as  $\text{C}_2\text{S}$ ,  $(\text{CaO})_3\text{SiO}_2$  as  $\text{C}_3\text{S}$ ,  $(\text{CaO})_3\text{Al}_2\text{O}_3$  as  $\text{C}_3\text{A}$  and  $(\text{CaO})_4(\text{Al}_2\text{O}_3)(\text{Fe}_2\text{O}_3)$  as  $\text{C}_4\text{AF}$ , where  $\text{C} = \text{CaO}$ ,  $\text{A} = \text{Al}_2\text{O}_3$ ,  $\text{S} = \text{SiO}_2$ , and  $\text{F} = \text{Fe}_2\text{O}_3$ .

We utilize the following assumptions: 1) the temperatures and pressure are homogeneously within each phase; 2) the dynamics along the width is ignored (2D); 3) no dust entrapped in the air; 4) thermal interactions with the environment and walls are ignored; and 5) only the 6 main clinker formation reactions are included.

#### A. Algebraic relations

The model consists of two sets of algebraic relations. 1) Thermo-physical relations between the specific energies,  $\hat{U}$ , and temperature, pressure, and concentration of each phase:

$$\hat{U}_a = \hat{H}_a - P\hat{V}_a = H_g(T_a, P, C_a) - PV_g(T_c, P, C_g), \quad (3a)$$

$$\hat{U}_s = \hat{H}_s = H_s(T_c, P, C_s). \quad (3b)$$

2) A geometric relation between the total specific volume of the gas and the solid phases:

$$\hat{V}_a + \hat{V}_s = V_a(T_a, P, C_a) + V_s(T_s, P, C_s) = \hat{V}_\Delta = 1. \quad (4)$$

#### B. Mass and Energy balances

The compound-specific mass balances of the solid and the air phases are

$$\partial_t C_{s,i} = -\nabla \cdot N_{s,i} + R_{s,i}, \quad (5a)$$

$$\partial_t C_{a,i} = -\nabla \cdot N_{a,i} + R_{a,i}, \quad (5b)$$

where  $i$  indicates the compound,  $N_{j,i}$  is the molar flux of phase  $j$ ,  $R_{j,i}$  is the production rate, and the divergence  $\nabla \cdot$  covers the dimensions  $y$  and  $z$ .

The energy balances of the solid and air phases are

$$\partial_t \hat{U}_s = -\nabla \cdot (\tilde{H}_s + \tilde{Q}_s) - \hat{Q}_{sa}^{rad} - \hat{Q}_{sa}^{cv} - J_{sa}, \quad (6)$$

$$\partial_t \hat{U}_a = -\nabla \cdot (\tilde{H}_a + \tilde{Q}_a) + \hat{Q}_{sa}^{rad} + \hat{Q}_{sa}^{cv} + J_{sa}, \quad (7)$$

where  $\tilde{H}_{j,i}$  is the enthalpy flux,  $\tilde{Q}_j$  is the thermal conduction,  $J_{sa}$  is the phase transition term and the specific heat transfer of radiation and convection is noted by  $\hat{Q}_{sa}^{rad}$  and  $\hat{Q}_{sa}^{cv}$ .

### C. Thermodynamic

Using thermo-physical models, we describe the enthalpy and volume of each phase by the functions  $H(T, P, n)$  and  $V(T, P, n)$ . For the mole vector,  $n$ , the models are homogeneous of order 1, and given as

$$H(T, P, n) = \sum_i n_i \left( \Delta H_{f,i}(T_0, P_0) + \int_{T_0}^T c_{p,i}(\tau) d\tau \right), \quad (8)$$

$$V(T, P, n) = \begin{cases} \frac{1}{1-\eta} \sum_i n_i \left( \frac{M_i}{\rho_i} \right), & \text{solid,} \\ \sum_i n_i \left( \frac{RT}{P} \right), & \text{air.} \end{cases} \quad (9)$$

$\Delta H_{f,i}(T_0, P_0)$  is the formation enthalpy at standard conditions  $(T_0, P_0)$ .  $\eta$  is the porosity of the clinker batch, giving the bulk volume. Assuming the clinkers are ideal spheres of equal size, the range of porosity [11] is

$$1 - \frac{\pi}{3\sqrt{2}} \leq \epsilon \leq 1. \quad (10)$$

In the literature, a constant porosity of 0.4 is used [3], though a more accurate porosity would depend on the clinker composition, e.g. sulfur content. The enthalpy density,  $\hat{H}$ , and volume density,  $\hat{V}$ , can be computed as

$$\hat{H}_s = H(T_s, P, C_s), \quad \hat{V}_s = V(T_s, P, C_s) \quad (11)$$

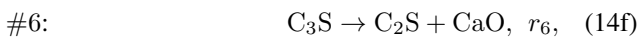
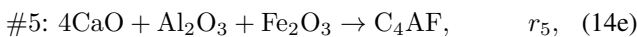
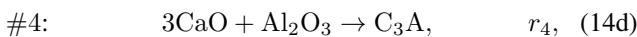
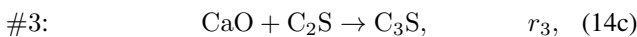
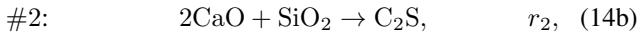
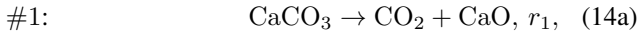
$$\hat{H}_a = H(T_a, P, C_a), \quad \hat{V}_a = V(T_a, P, C_a). \quad (12)$$

### D. Stoichiometry and kinetics

The production rates  $R$  in (5) are provided by the reaction rate vector  $r = r(T, P, C)$  and the stoichiometric matrix,  $\nu$ :

$$R = \begin{bmatrix} R_s \\ R_a \end{bmatrix} = \nu^T r. \quad (13)$$

$R_s$  and  $R_a$  are the production rate vectors of the clinker and air compounds respectively. The following reactions are considered:



The rate function  $r_j(T, P, C)$  is formulated as

$$r_j = k_r(T) \prod_l C_l^{\alpha_l}, \quad k(T) = k_r e^{-\frac{E_A}{RT}}. \quad (15)$$

$k(T)$  is the Arrhenius equation.  $C_l$  are the concentrations (mol/L).  $\alpha_l$  are the stoichiometric values. Table I shows the parameters for the kinetic expressions found in the literature. The heat transfer for phase transition,  $J_{sa}$ , is given as

$$J_{sa} = H(T_s, P, r_1). \quad (16)$$

### E. Transport

For each phase, mass is transported by advection, while energy is transported by advection, conduction, convection, and radiation.

TABLE I: Reaction rate coefficients.

Reactions	Units	$k_r$ [ $r_i$ ] · [ $C$ ] $^{-\Sigma\alpha}$	$E_A$ kJ/mol	$\alpha_1$	$\alpha_2$	$\alpha_3$
$r_1$	$\frac{\text{kg}}{\text{m}^3 \text{s}}$	$10^8$	175.7	1		
$r_2$	$\frac{\text{kg}}{\text{m}^3 \text{s}}$	$10^7$	240	2	1	
$r_3$	$\frac{\text{kg}}{\text{m}^3 \text{s}}$	$10^9$	420	1	1	
$r_4$	$\frac{\text{kg}}{\text{m}^3 \text{s}}$	$10^8$	310	3	1	
$r_5$	$\frac{\text{kg}}{\text{m}^3 \text{s}}$	$10^8$	330	4	1	1
$r_6$	$\frac{\text{kg}}{\text{s}^{-1}}$	$0.09^*$	$96.58^*$	1		

The reported units and coefficients of  $r_1$ - $r_5$  are from [12]. \* estimated coefficients of  $r_6$  using least-square and the Jander-data in [10].

1) *Material flux*: The mass transfer of each compound is driven by advection. The molar fluxes are

$$N_{s,i} = v_s C_{s,i}, \quad N_{a,i} = v_a C_{a,i}. \quad (17)$$

$v_j$  is the velocity vector.

2) *Enthalpy and heat transport*: The transport of energy includes the transport of enthalpy (advection) and thermal conduction (diffusion). The enthalpy flux,  $\tilde{H}$ , can be computed by

$$\tilde{H}_s = H(T_s, P, N_s), \quad \tilde{H}_a = H(T_a, P, N_a). \quad (18)$$

The thermal conduction is given by Fourier's law [13]

$$\tilde{Q}_s = -k_s \nabla T_s, \quad \tilde{Q}_a = -k_a \nabla T_a \quad (19)$$

with  $k_j$  being the thermal conductivity of the phase.

3) *Velocities*: Both the advection term of the material flux and the heat flux depend on the velocities in the cooler.

For the clinkers, we assume no dust is lifted by the airflow, so vertical movement is zero. The horizontal movement is given by the grate belt carrying the clinkers

$$v_s(z) = [v_{s,y}, v_{s,z}]^T = [0, v_{grate}(z)]^T. \quad (20)$$

For the air, the movement is driven by pressure differences and assumed independent of clinker and belt movements. We assume velocity is identical for each compound and is below 0.2 Mach in each direction. The velocities are given by the turbulent Darcy-Weisbach equation [14]:

$$v_a(y, z) = [v_{a,y}, v_{a,z}]^T, \quad (21)$$

$$v_{a,i} = \left( \frac{2}{0.316} \sqrt[4]{\frac{D_{H,i}^5 |\Delta P_i|}{\mu_a \rho_a^3 \Delta i}} \right)^{\frac{4}{7}} \text{sgn} \left( -\frac{\Delta P_i}{\Delta i} \right), \quad (22)$$

derived using the Darcy friction factor,  $f_D = 0.316 Re^{-\frac{1}{4}}$ .  $\mu_a$  is the air viscosity.  $\rho_a$  is the air density,

$$\rho_a = \frac{1}{\hat{V}_a} \sum_i M_i C_{a,i}. \quad (23)$$

$D_{H,i}$  is the hydraulic diameter for a non-uniform and non-circular cross-section channel [15],

$$D_{H,y} = \frac{4V_a}{2A_{yz} + 2A_{wy} + A_c}, \quad A_{wy} = w\Delta y, \quad (24)$$

$$D_{H,z} = \frac{4V_a}{2A_{yz} + 2A_{wz} + A_c}, \quad A_{wz} = w\Delta z, \quad (25)$$

$$A_{yz} = \Delta z \Delta y, \quad A_c = \frac{V_s}{\frac{\pi}{6} D_p^3} (\pi D_p^2). \quad (26)$$

$A_c$  is the total surface area of the clinkers.

4) *Heat transfer between phases:* The convective heat transfer between phases is given by Newton's law of heat transfer,

$$\hat{Q}_{sa}^{conv} = \hat{A}\beta(T_s - T_a). \quad (27)$$

The heat transfer due to thermal radiation is given by [3],

$$\hat{Q}_{sa}^{rad} = \hat{A}\sigma(\epsilon_s T_s^4 - \epsilon_a T_a^4). \quad (28)$$

$\hat{A}$  is the specific surface area.  $\sigma$  is the Stefan-Boltzmann's constant.  $\epsilon_s$  and  $\epsilon_a$  are the emissivity of each phase.  $\beta$  is the heat transfer coefficient [3]:

$$\hat{A} = \frac{6}{D_p}(1 - \hat{V}_a), \quad \beta = \frac{k_s Nu}{D_p + 0.5\phi D_p Nu}. \quad (29)$$

$\phi = 0.25$  is the clinker shape correction factor.  $D_p$  is the average clinker particle diameter, typically around 40 mm. The Nusselt Number  $Nu$  is given by

$$Nu = 2 + 1.8Pr^{\frac{1}{3}}Re^{\frac{1}{2}}, \quad (30)$$

$$Pr = \frac{c_{ps}\mu_a}{k_a}, \quad Re = \frac{\rho_a v_y D_p}{\mu_a}. \quad (31)$$

$Pr$  and  $Re$  is the Prandtl and Reynold number [3].  $\mu_a$  is the air viscosity. The heat capacity  $c_{ps}$  is given by:

$$c_{ps} = \sum_i n_i c_{m,i}. \quad (32)$$

$c_m$  is the molar heat capacity, shown in Table IV.

The emissivity of the clinker,  $\epsilon_s$ , can be assumed similar to the emissivity of clinker materials reported for the kiln,  $\epsilon_s = 0.9$  [16]. The emissivity of the air,  $\epsilon_a$ , is computed using the WSGG model of 4 grey gases [17],

$$\epsilon_g = \sum_{j=0}^4 a_j (1 - e^{-k_j S_m P(x_{H_2O} + x_{CO_2})}), \quad (33)$$

$$a_0 = 1 - \sum_{j=1}^4 a_j, \quad a_j = \sum_{i=1}^3 c_{j,i} \left(\frac{T}{T_{ref}}\right)^{i-1}, \quad (34)$$

$$k_j = K_{1,j} + K_{2,j} \frac{x_{H_2O}}{x_{CO_2}}, \quad x_i = \frac{n_i}{n_g}, \quad (35)$$

$$c_{j,i} = C_{1,j,i} + C_{2,j,i} \frac{x_{H_2O}}{x_{CO_2}} + C_{3,j,i} \left(\frac{x_{H_2O}}{x_{CO_2}}\right)^2. \quad (36)$$

$T_{ref}$  is 1200K.  $x_i$  is the molar fraction of  $CO_2$  or  $H_2O$ . The  $K$  and  $C$  coefficients are given by Table 1 in [17].  $S_m$  is the total path length. In this paper,  $S_m$  is taken as the distance between the centroids of the solid and gas phases,  $h/2$ , as an average length.

5) *Viscosity and conductivity:* In [18], the correlation between temperature and viscosity of a pure gas is given by

$$\mu_{a,i}(T) = \mu_0 \left(\frac{T}{T_0}\right)^{\frac{3}{2}} \frac{T_0 + S_{\mu,i}}{T + S_{\mu,i}}. \quad (37)$$

Table III provides the two measures of viscosity for calibrating  $S_{\mu,i}$ . A correlation between the air concentrations and the viscosity and thermal conductivity of a gas mixture

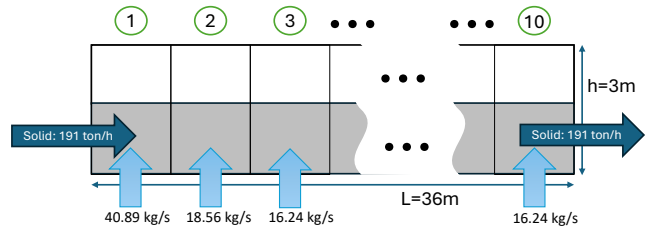


Fig. 3: Segment layout of the cooler with a selection of flows; solid flows (dark blue) and gas flows (light blue).

is provided by Wilke's formula [19] and the Mason-Saxena modified Wassiljewa's equation [20],

$$\mu_a = \sum_i \frac{x_i \mu_{a,i}}{\sum_j x_j \phi_{ij}}, \quad k_a = \sum_i \frac{x_i k_{a,i}}{\sum_j x_j \phi_{ij}}, \quad (38a)$$

$$\phi_{ij} = \left(1 + \sqrt{\frac{\mu_{a,i}}{\mu_{a,j}}} \sqrt{\frac{M_j}{M_i}}\right)^2 \left(2\sqrt{2} \sqrt{1 + \frac{M_i}{M_j}}\right)^{-1}. \quad (38b)$$

$x_i$  being the mole fraction of component  $i$

The thermal conductivity of the solid phase depends on the clinker composition and the porosity. Assuming the compounds can be considered as layers, the thermal conductivity is then given by the serial thermal conductivity [13],

$$\frac{1}{k_s} = \eta \frac{1}{k_a} + (1 - \eta) \sum_i \frac{V_{s,i}}{V_s} \frac{1}{k_{s,i}}, \quad (39)$$

where the width ratio is represented by a volume ratio.

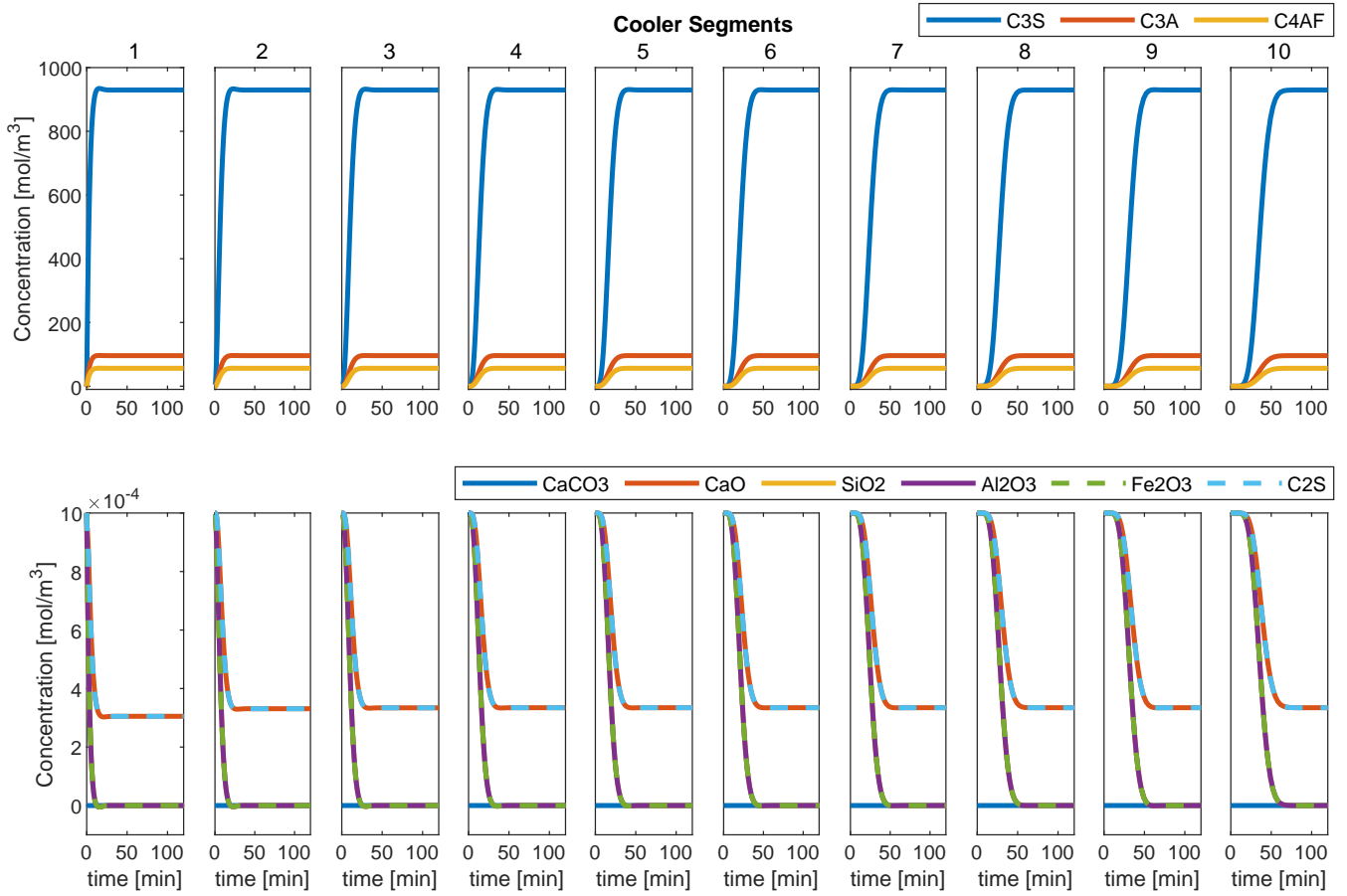
Table II and III show the material data of each compound.

#### F. boundary conditions

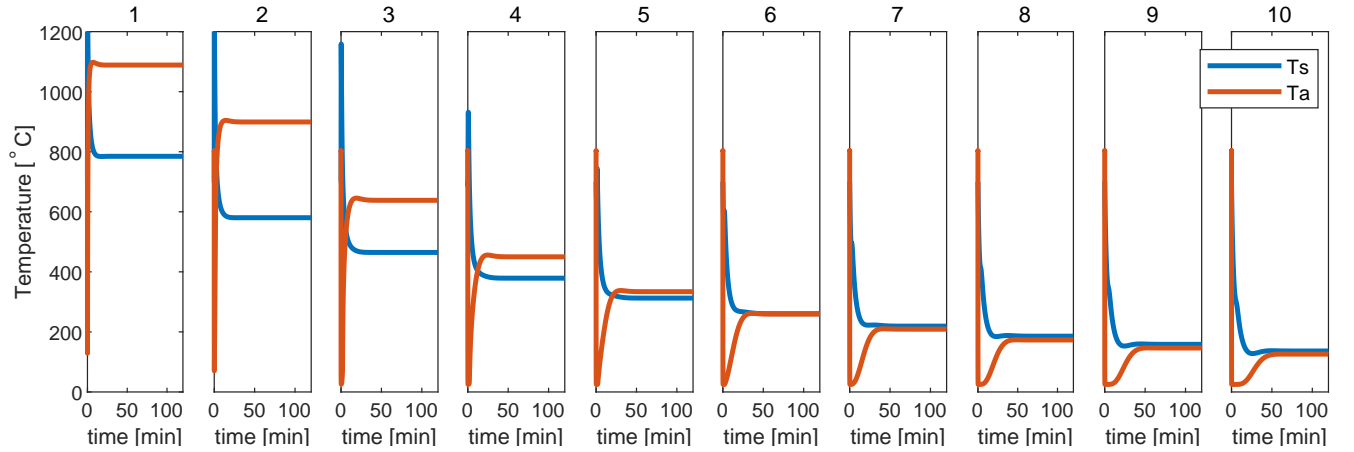
The model is bounded by the following variables. 1) the molar flux of air blown in by the fans below the grate belt; 2) the molar influx of clinker compounds; 3) the external pressures; the kiln, 3rd air duct, and environment pressure; 4) the location of the connections to neighboring units; i.e. which segment is connected to which external pressure.

#### IV. SIMULATION RESULTS

To demonstrate the simulation model, we simulate the cooler for 2 hours of operation. A steady-state simulation from FLSmidth Cement is used for comparison. We consider a 36 m long cooler with 4 m width and 3 m tall. We use a 10-segment model, as illustrated in Fig. 3. The operation is set to a 191 ton/h clinker production. The clinker inflow composition is 79.96%  $C_3S$ , 9.76%  $C_3A$ , and 10.28%  $C_4AF$  with a temperature of 1450°C. The grate belts were run uniformly with a residence time of 36 min, 0.017 m/s. The air inflows for each segment are 40.89 kg/s for the first, 18.56 kg/s for the second, and 16.24 kg/s for the remaining segments. The inflow is regular air with 1%  $H_2O$  vapor at 25°C. The ambient pressure is 1.01325 bar (1 atm), the kiln pressure is 1.0115 bar, and the 3rd air pressure is 1.01125 bar. The kiln pressure is set on segment 1, the 3rd air pressure is set on segment 2, and the ambient pressure covers the remaining segments. We used a uniform clinker concentration of 10 mol/m<sup>3</sup> at 700°C for initialization, with the air being



(a) Evolution of the concentration of clinker components in the cooler.



(b) Evolution of the solid and air temperatures in the cooler.

Fig. 4: Dynamic simulation of cooler concentration and temperature. The cooler is divided into 10 segments of finite volumes.

800°C. The specific scenario was chosen to clearly highlight the dynamic aspects of the model, e.g.  $C_3S$  decomposition, thus the 79.96%  $C_3S$  complete reaction scenario instead of the typical 60-70% range with the corresponding  $C_2S$  and  $CaO$  present.

#### A. Model calibration

The Darcy friction factor  $f_D$  is manually calibrated to fit the expected pressure drop in the reference simulation. To

obtain a drop of 1.06 bar to 1.015 bar, a factor of 100 is used; representing a less smooth scenario of gas movement.

#### B. Dynamic performance

Fig. 4 illustrates the dynamic behavior of the model. Fig. 4a shows the solid molar concentrations and Fig. 4b shows the temperature. We observe the system settles to a steady state after 50-60 min, with the first segment settling around 20 min. The concentrations increase monotonically as the

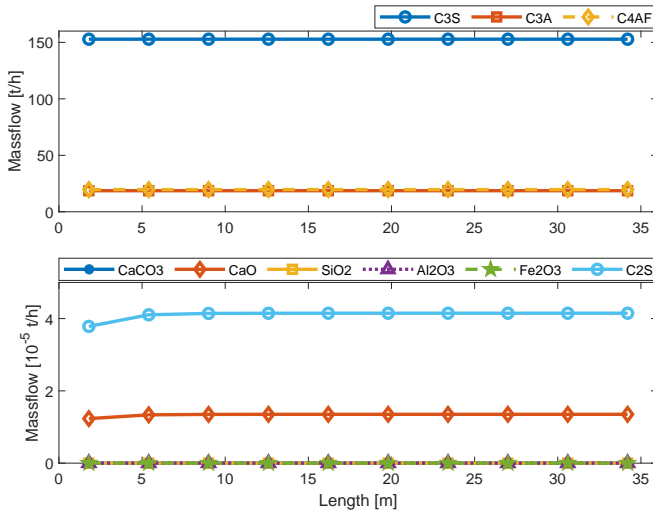


Fig. 5: The steady-state mass flows of solids along the length of the cooler. All of the decomposition of Alite ( $C_3S$ ) to Belite ( $C_2S$ ) is quickly halted by the cooling.

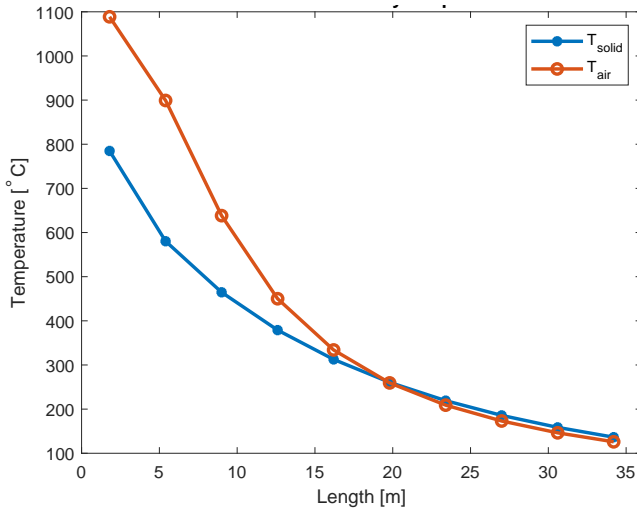


Fig. 6: The steady-state temperature of the clinker mass and air content in the cooler.

clinker flows in except  $C_3S$ , which has slight overshoots of up to  $2 \text{ mol/m}^3$  due to the decomposition of Alite. We observe that the initial temperatures in Fig. 4b drop rapidly and then increase as the material influx wave arrives.

### C. Steady-state results

Fig. 5 shows the steady-state mass flow of the clinker compounds. The mass flow of  $C_2S$  and  $CaO$  shows slight increases from their zero inflow, indicating  $C_3S$  decomposition. Confirming the  $C_3S$  overshoot is due to decomposition. Fig. 6 shows the steady-state temperature profile of the cooler. The air temperature of segment 1 is  $1088.7^\circ\text{C}$  matching the  $1089^\circ\text{C}$  for 2nd air flows. The air temperature of segment 2 is  $899.1^\circ\text{C}$  comparable to the  $968^\circ\text{C}$  for 3rd air flows. The solid temperature at segment 1 is  $784.8^\circ\text{C}$  below the decomposition range. In segment 2, the temperature at  $580.3^\circ\text{C}$  is

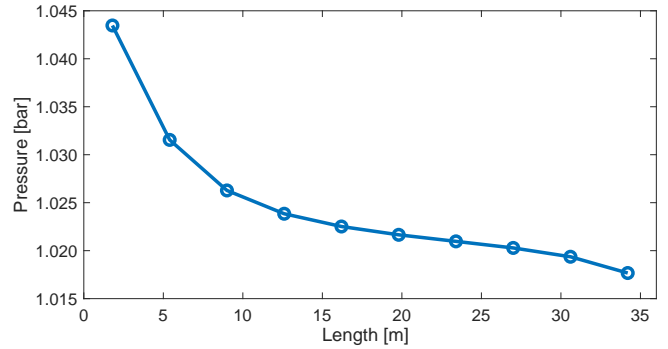


Fig. 7: The steady-state pressure profile in the cooler.

well below the range, thus halting the  $C_3S$  decomposition. By extrapolating the slope of the solid temperature, the outlet clinker temperature is estimated to  $125.3^\circ\text{C}$ , which fits within the temperature range of the outlet clinker,  $100 - 150^\circ\text{C}$  [7]. Fig. 7 shows the steady-state pressure profile. The pressure of segment 1 lies in between the kiln pressure and inflow pressure (1.06 bar), with the pressure throughout the cooler decreasing towards the ambient pressure.

## V. CONCLUSION

In this paper, we modeled a cooler in a cement plant's pyro-section as an index-1 DAE model. The model is constructed using a systematic modeling approach involving thermo-physical properties, transport phenomena, stoichiometry and kinetics, mass and energy balances, and algebraic relations for the volume and internal energy. A model simulation illustrating the cooler dynamics is provided, including the cooling aspects and the decomposition of Alite. The simulation is shown to match the reference operation qualitatively.

The utility of the cooler model covers both dynamic and steady-state simulation. For dynamic simulations of the full pyro-section, the cooler model will be connected to modules for the rotary kiln, the calciner, and the pre-heating cyclones. The model allows for the prediction and evaluation of operation strategies and serves as a basis for improving clinker quality and energy efficiency through optimization, i.e., the cooling rate.

## REFERENCES

- [1] J. Lehne and F. Preston, "Making concrete change: Innovation in low-carbon cement and concrete," Chatham House, Tech. Rep., June 2018.
- [2] M. Metzger, "Simplified mathematical model of the rotary kiln unit dynamical properties," *IFAC Proceedings Volumes*, vol. 16, no. 10, pp. 491–497, 1983.
- [3] Z. Cui, W. Shao, Z. Chen, and L. Cheng, "Mathematical model and numerical solutions for the coupled gas–solid heat transfer process in moving packed beds," *Applied Energy*, vol. 206, pp. 1297–1308, 2017.
- [4] K. S. Mujumdar, K. Ganesh, S. B. Kulkarni, and V. V. Ranade, "Rotary cement kiln simulator (RoCKS): Integrated modeling of pre-heater, calciner, kiln and clinker cooler," *Chem. Eng. Sci.*, vol. 62, no. 9, pp. 2590–2607, 2007.
- [5] J. L. Svendsen, W. R. L. da Silva, J. P. Merino, D. Sampath, and J. B. Jørgensen, "A dynamical simulation model of a cement clinker rotary kiln," in *European Control Conference 2024*, 2024, pp. 1–7.

[6] J. L. Svendsen, W. R. L. da Silva, and J. B. Jørgensen, "A first-engineering principles model for dynamical simulation of a calciner in cement production," in *12th IFAC Symposium on Advanced Control of Chemical Processes (ADCHEM 2024)*, 2024, pp. 1–7.

[7] J. Bhatti, F. Macgregor Miller, and S. H. Kosmatka, *Innovations in Portland Cement Manufacturing*. Portland Cement Association, 2010.

[8] A. Chatterjee, *Cement Production Technology: Principles and Practice*. CRC Press, 2018.

[9] G. Bye, *Portland Cement: Composition, Production and Properties*. Thomas Telford, 1999.

[10] X. Li, X. Shen, M. Tang, and X. Li, "Stability of tricalcium silicate and other primary phases in portland cement clinker," *Ind. Eng. Chem. Res.*, vol. 53, no. 5, pp. 1954–1964, 2014.

[11] T. Hales, M. Adams, G. Bauer, T. D. Dang, J. Harrison, L. T. Hoang, C. Kaliszky, V. Magron, S. Mclaughlin, T. T. Nguyen, Q. T. Nguyen, T. Nipkow, S. Obua, J. Pleso, J. Rute, A. Solovyev, T. H. A. Ta, N. T. Tran, T. D. Trieu, J. Urban, K. Vu, and R. Zumkeller, "A formal proof of the kepler conjecture," *Forum of Math. Pi*, vol. 5, p. e2, 2017.

[12] E. Mastorakos, A. Massias, C. D. Tsakiroglou, D. A. Goussis, V. N. Burganos, and A. C. Payatakes, "CFD predictions for cement kilns including flame modelling, heat transfer and clinker chemistry," *Applied Mathematical Modelling*, vol. 23, pp. 55–76, 1999.

[13] D. W. Green and R. H. Perry, Eds., *Perry's Chemical Engineers' Handbook*, 8th ed. McGraw Hill, 2008.

[14] G. W. Howell and T. M. Weathers, *Aerospace Fluid Component Designers' Handbook. Vol. I, Rev. D*. TRW Systems Group, 1970.

[15] J. E. Hesselgreaves, R. Law, and D. A. Reay, "Chapter 1 - introduction," in *Compact Heat Exchangers*, 2nd ed. Butterworth-Heinemann, 2017, pp. 1–33.

[16] T. Hanein, F. P. Glasser, and M. N. Bannerman, "One-dimensional steady-state thermal model for rotary kilns used in the manufacture of cement," *Adv. Appl. Ceram.*, vol. 116, no. 4, pp. 207–215, 2017.

[17] R. Johansson, B. Leckner, K. Andersson, and F. Johnsson, "Account for variations in the H<sub>2</sub>O to CO<sub>2</sub> molar ratio when modelling gaseous radiative heat transfer with the weighted-sum-of-grey-gases model," *Combustion and Flame*, vol. 158, pp. 893–901, 2011.

[18] W. Sutherland, "The Viscosity of Gases and Molecular Force," *Philos Mag series 5*, vol. 36, no. 223, pp. 507–531, 1893.

[19] C. R. Wilke, "A viscosity equation for gas mixtures," *The Journal of Chemical Physics*, vol. 18, no. 4, pp. 517–519, 1950.

[20] B. E. Poling, J. M. Prausnitz, and J. P. O'Connell, *The Properties of Gases and Liquids*. McGraw-Hill, 2001.

[21] J. Rumble, Ed., *CRC handbook of chemistry and physics*, 103rd ed. CRC Press, 2022.

[22] A. Ichim, C. Teodoriu, and G. Falcone, "Estimation of cement thermal properties through the three-phase model with application to geothermal wells," *Energies*, vol. 11, no. 10, 2018.

[23] M. J. Abdolhosseini Qomi, F.-J. Ulm, and R. J.-M. Pellenq, "Physical origins of thermal properties of cement paste," *Phys. Rev. Appl.*, vol. 3, p. 064010, Jun 2015.

[24] Y. Du and Y. Ge, "Multiphase model for predicting the thermal conductivity of cement paste and its applications," *Materials*, vol. 14, no. 16, 2021.

[25] G. C. Bye, Ed., *Portland Cement: Composition, Production and Properties*, 2nd ed. Thomas Telford, 1999.

[26] T. Hanein, F. P. Glasser, and M. N. Bannerman, "Thermodynamic data for cement clinkering," *Cem. Concr. Res.*, vol. 132, p. 106043, 2020.

## APPENDIX

### VI. MATERIAL PROPERTIES

Table II and Table III shows literature data for the material properties of the compounds for the solid and air phases. Table IV reports the parameters ( $C_0$ ,  $C_1$ ,  $C_2$ ) for computing the specific heat capacities of the components [5],

$$c_p = C_0 + C_1T + C_2T^2. \quad (40)$$

TABLE II: Material properties of the solid phase

Units	Thermal Conductivity	Density	Molar mass
	$\frac{W}{K m}$	$\frac{g}{cm^3}$	$\frac{g}{mol}$
CaCO <sub>3</sub>	2.248 <sup>a</sup>	2.71 <sup>b</sup>	100.09 <sup>b</sup>
CaO	30.1 <sup>c</sup>	3.34 <sup>b</sup>	56.08 <sup>b</sup>
SiO <sub>2</sub>	1.4 <sup>a,c</sup>	2.65 <sup>b</sup>	60.09 <sup>b</sup>
Al <sub>2</sub> O <sub>3</sub>	12-38.5 <sup>c</sup> 36 <sup>a</sup>	3.99 <sup>b</sup>	101.96 <sup>b</sup>
Fe <sub>2</sub> O <sub>3</sub>	0.3-0.37 <sup>c</sup>	5.25 <sup>b</sup>	159.69 <sup>b</sup>
C <sub>2</sub> S	3.45±0.2 <sup>d</sup>	3.31 <sup>d</sup>	172.24 <sup>g</sup>
C <sub>3</sub> S	3.35±0.3 <sup>d</sup>	3.13 <sup>d</sup>	228.32 <sup>b</sup>
C <sub>3</sub> A	3.74±0.2 <sup>e</sup>	3.04 <sup>b</sup>	270.19 <sup>b</sup>
C <sub>4</sub> AF	3.17±0.2 <sup>e</sup>	3.7-3.9 <sup>f</sup>	485.97 <sup>g</sup>

<sup>a</sup> from [13], <sup>b</sup> from [21], <sup>c</sup> from [22], <sup>d</sup> from [23], <sup>e</sup> from [24], <sup>f</sup> from [25], <sup>g</sup> Computed from the above results

TABLE III: Material properties of the gas phase

Units	Thermal Conductivity <sup>a</sup>	Molar mass <sup>a</sup>	Viscosity <sup>a</sup>
	$\frac{10^{-3}W}{K m}$	$\frac{g}{mol}$	$\mu Pa s$
CO <sub>2</sub>	16.77 (T=300K)	44.01	15.0 (T=300K)
	70.78 (T=1000K)		41.18 (T=1000K)
N <sub>2</sub>	25.97(T=300K)	28.014	17.89(T=300K)
	65.36(T=1000K)		41.54(T=1000K)
O <sub>2</sub>	26.49(T=300K)	31.998	20.65 (T=300K)
	71.55(T=1000K)		49.12 (T=1000K)
Ar	17.84 (T=300K)	39.948	22.74(T=300K)
	43.58 (T=1000K)		55.69(T=1000K)
CO	25(T=300K)	28.010	17.8(T=300K)
	43.2(T=600K)		29.1(T=1000K)
H <sub>2</sub> O	609.50(T=300K)	18.015	853.74(T=300K)
	95.877(T=1000K)		37.615(T=1000K)
H <sub>2</sub>	193.1 (T=300K)	2.016	8.938(T=300K)
	459.7 (T=1000K)		20.73 (T=1000K)

<sup>a</sup> from [21], <sup>b</sup> from [20]

TABLE IV: Molar heat capacity

Units	$C_0$	$C_1$	$C_2$	Temperature range
	$\frac{J}{mol \cdot K}$	$\frac{10^{-3}J}{mol \cdot K^2}$	$\frac{10^{-5}J}{mol \cdot K^3}$	K
CaCO <sub>3</sub> <sup>a</sup>	23.12	263.4	-19.86	300-600
CaO <sup>b</sup>	71.69	-3.08	0.22	200 - 1800
SiO <sub>2</sub> <sup>b</sup>	58.91	5.02	0	844 - 1800
Al <sub>2</sub> O <sub>3</sub> <sup>b</sup>	233.004	-19.5913	0.94441	200 - 1800
Fe <sub>2</sub> O <sub>3</sub> <sup>a</sup>	103.9	0	0	-
C <sub>2</sub> S <sup>b</sup>	199.6	0	0	1650 - 1800
C <sub>3</sub> S <sup>b</sup>	333.92	-2.33	0	200 - 1800
C <sub>3</sub> A <sup>b</sup>	260.58	9.58/2	0	298 - 1800
C <sub>4</sub> AF <sup>b</sup>	374.43	36.4	0	298 - 1863
CO <sub>2</sub> <sup>a</sup>	25.98	43.61	-1.494	298 - 1500
N <sub>2</sub> <sup>a</sup>	27.31	5.19	-1.553e-04	298 - 1500
O <sub>2</sub> <sup>a</sup>	25.82	12.63	-0.3573	298 - 1100
Ar <sup>a</sup>	20.79	0	0	298 - 1500
CO <sup>a</sup>	26.87	6.939	-0.08237	298 - 1500
H <sub>2</sub> O <sup>a</sup>	30.89	7.858	0.2494	298 - 1300
H <sub>2</sub> <sup>a</sup>	28.95	-0.5839	0.1888	298 - 1500

<sup>a</sup> based on data from [21], <sup>b</sup> coefficients from [26]